The rRNA methyltransferase Bud23 shows functional interaction with components of the SSU processome and RNase MRP

RICHA SARDANA, JOSHUA P. WHITE, and ARLEN W. JOHNSON[1]

Section of Molecular Genetics and Microbiology and the Institute for Cellular and Molecular Biology, The University of Texas at Austin, Austin, Texas 78712, USA

ABSTRACT

Bud23 is responsible for the conserved methylation of G1575 of 18S rRNA, in the P-site of the small subunit of the ribosome. *bud23Δ* mutants have severely reduced small subunit levels and show a general failure in cleavage at site A2 during rRNA processing. Site A2 is the primary cleavage site for separating the precursors of 18S and 25S rRNAs. Here, we have taken a genetic approach to identify the functional environment of *BUD23*. We found mutations in *UTP2* and *UTP14*, encoding components of the SSU processome, as spontaneous suppressors of a *bud23Δ* mutant. The suppressors improved growth and subunit balance and restored cleavage at site A2. In a directed screen of 50 ribosomal *trans*-acting factors, we identified strong positive and negative genetic interactions with components of the SSU processome and strong negative interactions with components of RNase MRP. RNase MRP is responsible for cleavage at site A3 in pre-rRNA, an alternative cleavage site for separating the precursor rRNAs. The strong negative genetic interaction between RNase MRP mutants and *bud23Δ* is likely due to the combined defects in cleavage at A2 and A3. Our results suggest that Bud23 plays a role at the time of A2 cleavage, earlier than previously thought. The genetic interaction with the SSU processome suggests that Bud23 could be involved in triggering disassembly of the SSU processome, or of particular subcomplexes of the processome.

Keywords: ribosome biogenesis; methyltransferase; SSU processome; RNase MRP; Bud23; A2 cleavage

INTRODUCTION

Eukaryotic ribosomes consist of two subunits—the small (40S) and the large (60S) subunits. The biogenesis of both subunits is a highly ordered and complex process that begins in the nucleolus with the transcription of the polycistronic 35S pre-rRNA by RNA polymerase I (Warner 2001; Panse and Johnson 2010). The 35S pre-RNA undergoes a series of successive, regulated, and specific modifications and cleavages required to produce 18S, 25S, and 5.8S rRNAs present in the mature ribosome (Fromont-Racine et al. 2003; Henras et al. 2008).

Factors involved in small subunit biogenesis associate co- and post-transcriptionally with the pre-rRNA transcript (Granneman and Baserga 2005). The earliest of these factors, along with U3 snoRNA, form the SSU (small subunit) processome and are required for the critical cleavages of rRNA at A0, A1 in the 5′-external transcribed spacer (ETS), and at A2 in internal transcribed spacer 1 (ITS1) (Dragon et al. 2002; Grandi et al. 2002; Granneman and Baserga 2004; Henras et al. 2008). The U3 snoRNP–pre-rRNA complex or the SSU processome has also been referred to as the 90S pre-ribosome (Schafer et al. 2003). The SSU processome, in turn, is composed of several subcomplexes, namely, the UTP-A, UTP-B, UTP-C, MPP10, and the BMS1 subcomplexes (Granneman and Baserga 2004). The timely and hierarchical association of each of these subcomplexes with the nascent transcript has been shown to be critical for the proper maturation of the ribosome (Venema and Tollervey 1999; Henras et al. 2008).

The rRNA processing complexes containing U3 snoRNA can be seen cotranscriptionally associated with the nascent pre-rRNA transcript as 5′-terminal knobs in electron micrographs of Miller chromatin spreads (Mougey et al. 1993; Dragon et al. 2002; French et al. 2003; Gallagher et al. 2004; Osheim et al. 2004). The terminal knobs are dynamic entities that begin as small knobs and then condense into larger knobs as more factors join and the rRNA is folded into a more compact structure (Dragon et al. 2002; Wery et al. 2009). This is accompanied by cotranscriptional modifications

Abbreviations: SSU processome, small subunit processome; IP, immunoprecipitation; TEV protease, tobacco etch virus protease; YFEG, You Favorite Essential Gene; snoRNA, small nucleolar RNA; rRNA, ribosomal RNA; GFP, green fluorescent protein; TAP, tandem affinity purification; ETS, external transcribed spacer; ITS, internal transcribed spacer; PMSF, phenylmethylsulfonyl fluoride; TCA, trichloroacetic acid; IgG, immunoglobulin G; ts, temperature sensitive.

[1]**Corresponding author**

E-mail arlen@austin.utexas.edu

Article published online ahead of print. Article and publication date are at http://www.rnajournal.org/cgi/doi/10.1261/rna.037671.112.

and cleavage at A0 and A1 in the 5′ ETS. Subsequent cleavage at A2 in ITS1 separates the small and large subunit biogenesis pathways (Osheim et al. 2004; Kos and Tollervey 2010). The cleavage at A2 in the canonical processing pathway generates 20S pre-rRNA. However, A2 cleavage is not obligatory; pre-rRNA can be cleaved in ITS1 at site A3 instead of at A2, generating the normal 27SA3 intermediate (Torchet and Hermann-Le Denmat 2000; Vos et al. 2004). Cleavage at A3 is carried out by the endonuclease activity of the RNase MRP ribonucleoprotein complex (Torchet and Hermann-Le Denmat 2000). Many SSU processome–associated accessory factors and U3 snoRNA leave the pre-40S ribosome at this stage, which may coincide with release of the pre-40S from the nucleolus (Schafer et al. 2003). Additional accessory factors required for late maturation events along with several ribosomal proteins join the pre-40S prior to export to the cytoplasm. 20S pre-rRNA in the pre-40S particles is cleaved at site D in the cytoplasm to form 18S rRNA, the mature rRNA in 40S subunits (Vanrobays et al. 2003).

We previously characterized Bud23 as a protein important for the biogenesis and nuclear export of 40S ribosomal subunits in *Saccharomyces cerevisiae* (White et al. 2008). Based on sequence homology and predicted structure analysis, Bud23 was identified as the methyltransferase responsible for m7G1575 in the P-site of the decoding center (White et al. 2008). Despite the position of this base in a critical location of the subunit, it is the presence of Bud23 protein but not its methyl transferase activity that is important for 40S biogenesis (White et al. 2008). More recently, work from our and the Lafontaine group identified Trm112 as a cofactor required for the stability of Bud23 in vivo (Figaro et al. 2012; Sardana and Johnson 2012). In this study, we have further addressed the role of Bud23 in 40S subunit biogenesis. We show that Bud23 is important for efficient A2 cleavage and shows genetic interactions with several SSU components and suggest that it plays a role in triggering SSU processome disassembly.

RESULTS

BUD23 physically interacts with middle-stage 40S biogenesis factors

In an attempt to understand what role *BUD23* plays in small subunit biogenesis, we first mapped the association of Bud23 with nascent ribosomes in the known sequential pathway of accessory factor binding in 40S biogenesis (Dez and Tollervey 2004). A plasmid harboring C-terminal GFP-tagged Bud23 was transformed into strains expressing genomic C-terminal TAP-tagged factors acting at early (Utp9, Utp18, Utp22, Utp25), middle (Enp1, Nob1, Hrr25, Ltv1), and late (Rio2, Hcr1) stages of small subunit biogenesis (Dez and Tollervey 2004). Affinity purification was performed using the TAP tag, and the immunoprecipitates were probed for Bud23-GFP and for Rps8 as a marker for 40S. Bud23-GFP coimmunoprecipitated with biogenesis factors that work in the middle stages of small subunit biogenesis (Enp1, Nob1, Hrr25, and Ltv1) but not with early (Utp9, Utp18, Utp22, Utp25) or late cytoplasmic 40S associated factors (Rio2, Hcr1) (Fig. 1A). Because we have previously observed that a C-terminal GFP-tag partially impairs Bud23 function (Li et al. 2009), we repeated this analysis with an N-terminally tagged construct and obtained similar results (data not shown).

To ascertain which RNA intermediates interact most stably with Bud23-associated complexes, we performed immunoprecipitation using C-terminal TAP-tagged Bud23. Bud23-TAP efficiently pulled down 20S pre-rRNA, but not 35S pre-rRNA or U3 snoRNA, RNAs that are associated with the Utp proteins including Utp9 (Fig. 1B,C; Dragon et al. 2002; Grandi et al. 2002). These results of RNAs associated with Bud23 were consistent with the results of protein copurification: that Bud23 is recruited to the pre-40S pathway at an intermediate step in the nucleolus and/or nucleus, but is not present in the earliest SSU-containing particles or late cytoplasmic pre-40S. We conclude that Bud23 joins the pre-ribosome near the transition from the early U3 snoRNP-bound 90S particle to the 20S rRNA containing pre-40S particle.

Genetic interactions of *BUD23*

bud23Δ shows negative genetic interaction with UTP-A and RNase MRP components

Although physical interactions give information about stable interactions, genetic interactions can reveal functional inter-

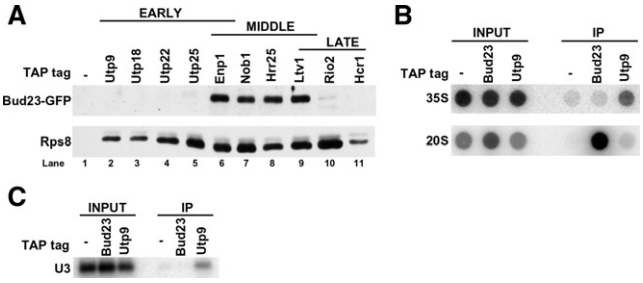

FIGURE 1. Bud23 stably associates with middle-stage factors of small-subunit maturation. (*A*) Bud23-GFP immunoprecipitates with middle-stage-acting biogenesis factors. Extracts from cells expressing the indicated C-terminal TAP-tagged 40S biogenesis factors and Bud23-GFP (pAJ2151) were immunoprecipitated with IgG-Sepharose. Extracts from cells expressing only Bud23-GFP were used as negative control. Immunoprecipitated proteins were subjected to SDS-PAGE and Western blotting using anti-GFP-HRP and anti-Rps8 antibodies to detect Bud23-GFP and Rps8, respectively. (*B*) Bud23-TAP immunoprecipitates 20S pre-rRNA. Extracts from cells expressing Bud23-TAP (pAJ2558) were immunoprecipitated with IgG-Sepharose. Extracts prepared from cells expressing untagged Bud23 and Utp9-TAP were used as negative and positive controls, respectively. Immunoprecipitated RNA was analyzed for the presence of 35S and 20S rRNA by dot blotting using oligos listed in Table 5. (*C*) Bud23-TAP does not immunoprecipitate U3 snoRNA. Extracts from cells expressing Bud23-TAP were immunoprecipitated with IgG-Sepharose. Extracts prepared from cells expressing untagged Bud23 and Utp9-TAP were used as negative and positive controls, respectively. Immunoprecipitated RNA was analyzed for the presence of U3 snoRNA by Northern blotting with AJO1686 listed in Table 5.

TABLE 1. Negative genetic interactions

Known function	Strain	Fitness at 31°C	Expected fitness for no interaction	Observed fitness	% fitness reduction from expected
		Single mutant	*yfeg-ts::URA3 bud23Δ::KanMX Double mutant*		
	WT	1			
	bud23Δ	0.47			
SSU processome associated	*dhr2*	0.31	0.15	0.1	33%
SSU processome associated	*utp8*	0.57	0.27	0.097	64%
SSU processome associated	*utp9*	0.6	0.28	<0.04	>86%
SSU processome associated	*utp12*	0.56	0.26	0.14	46%
SSU processome associated	*utp24*	0.69	0.33	0.21	34%
SSU processome associated	*emg1*	0.66	0.27	0.15	44%
H/ACA snoRNP associated	*nhp2*	0.42	0.2	0.12	42%
RNase MRP	*pop3*	0.33	0.155	0.08	48%
RNase MRP	*pop4*	0.49	0.23	0.138	40%
RNase MRP	*snm1*	0.41	0.19	<0.04	>79%
Ribosomal protein	*rps13*	0.74	0.35	0.2	43%
rRNA transcription	*reb1*	0.56	0.26	0.11	58%
rRNA transcription	*rrn7*	0.68	0.32	0.13	59%
Nucleocytoplasmic transport	*srp1*	0.69	0.33	0.09	73%
Nucleocytoplasmic transport	*ntf2*	0.46	0.23	0.08	65%

actions. Therefore, we decided to test for genetic interactions with the *bud23Δ* mutant. Biogenesis of eukaryotic ribosomal subunits is dependent on more than 200 accessory factors (Henras et al. 2008), a large percentage of which are essential. We took advantage of a temperature-sensitive (ts) collection consisting of approximately 250 essential genes in *S. cerevisiae* (Ben-Aroya et al. 2008). Each mutant in this collection is marked with a *URA3* gene: *yfeg-ts-URA3* (your favorite essential gene, YFEG). We selected 50 ts mutants from this collection that were reported to have rRNA processing defects (Ben-Aroya et al. 2008). Each of these ts mutant strains was crossed to a *bud23Δ* mutant. Haploid double mutants (*yfeg-ts-URA3 bud23Δ*::*KanMX*) were then assayed for genetic interaction by comparing the growth of the double mutant with the parental single mutants. The doubling times and growth curves for each strain were generated as described (Toussaint and Conconi 2006). We scored neutral genetic interactions as having the fitness predicted by the product of the fitness of individual mutants. Positive genetic interactions were indicated by fitness deficits less than predicted from the product of the individual parental fitness, whereas synthetic negative genetic interactions were indicated by fitness deficits greater than the simple product of the individual mutants (Dixon et al. 2009).

We identified multiple negative and positive interactions in our genetic screen (Tables 1, 2). Strong negative genetic interactions with *bud23Δ* were observed with a few functionally revealing clusters. The first cluster was composed of SSU

TABLE 2. Positive genetic interactions

Known function	Strain	Fitness at 33°C	Expected fitness for no interaction	Observed fitness	% fitness increase from expected
		Single mutant	*yfeg-ts::URA3 bud23Δ::KanMX Double mutant*		
	WT	1			
	bud23Δ	0.43			
tRNA methylation	*trm5*	0.43	0.18	0.49	63%
SSU processome associated	*utp18*	0.65	0.28	0.51	45%
SSU processome associated	*enp2*	0.55	0.24	0.41	41%
Intranuclear transport	*noc2*	0.15	0.064	0.24	73%
DNA repair and SSU biogenesis	*hrr25*	0.4	0.18	0.29	39%
Late SSU maturation	*tsr4*	0.075	0.032	0.091	65%
Late SSU maturation	*nob1*	0.53	0.22	0.42	48%
Translation Initiation	*rpg1*	0.54	0.24	0.46	48%
Spliceosome disassembly	*ntr2*	0.6	0.26	0.43	40%
Chromatic remodeling	*fmp47*	0.42	0.18	0.41	56%
CoA biosynthesis	*cab5*	0.11	0.05	0.35	86%
Function unknown	*ylr132c*	0.44	0.19	0.43	56%

processome components, notably the UTP-A complex members Utp8 and Utp9. The UTP-A complex has been reported to be the earliest protein subcomplex of the SSU processome that binds cotranscriptionally to the nascent pre-rRNA (Gallagher et al. 2004; Henras et al. 2008). A second category of strong negative genetic interactions was observed with components of the RNase MRP ribonucleoprotein complex: Snm1, Pop3, and Pop4. RNase MRP is an essential ribonucleoprotein complex that is responsible for cleavage at site A3 in ITS1 (Lygerou et al. 1996). Negative genetic interaction was also observed with Dhr2, Utp12, Utp24, and Emg1 (all SSU processome–associated proteins), Nhp2 (a protein essential for H/ACA snoRNP function), Reb1 and Rrn7 (RNA polymerase I–associated proteins), Srp1 and Ntf2 (proteins involved in nucleo-cytoplasmic transport), and ribosomal protein Rps13 (Table 1).

Several proteins known to be involved in various stages of small-subunit biogenesis—Utp18, Enp2, Tsr4, Hrr25, and Nob1—exhibited positive genetic interaction with *BUD23*. We also identified positive genetic interactions with genes that have no known role in 40S biogenesis: *TRM5*, *NTR2*, *NOC2*, *RPG1*, *FMP47*, *CAB5*, and *YLR132c* (Table 2). The genetic interactions with the SSU processome and RNase MRP components were particularly interesting and suggest that Bud23 plays an earlier role in 40S biogenesis than is obvious from physical interactions.

The *bud23Δ* growth defect is suppressed by mutations in SSU processome components

Although *BUD23* is not essential for viability, deletion of the gene results in a severe slow-growth phenotype (Fig. 2A; Tables 1, 2; White et al. 2008). We took advantage of the slow growth rate of a *bud23Δ* mutant to isolate spontaneous extragenic suppressors. All such suppressors that we identified were dominant (data not shown). We analyzed two of these suppressors (see Materials and Methods) and identified single amino acid changes in Utp14 (A758G) and in Utp2 (A2D). Utp2 is also named Nop14. These mutations strongly suppressed the growth defect and 40S subunit deficit of a *bud23Δ* mutant (Fig. 2A,B), although levels were not fully restored to those of wild type. Epitope-tagged mutant Utp14 and

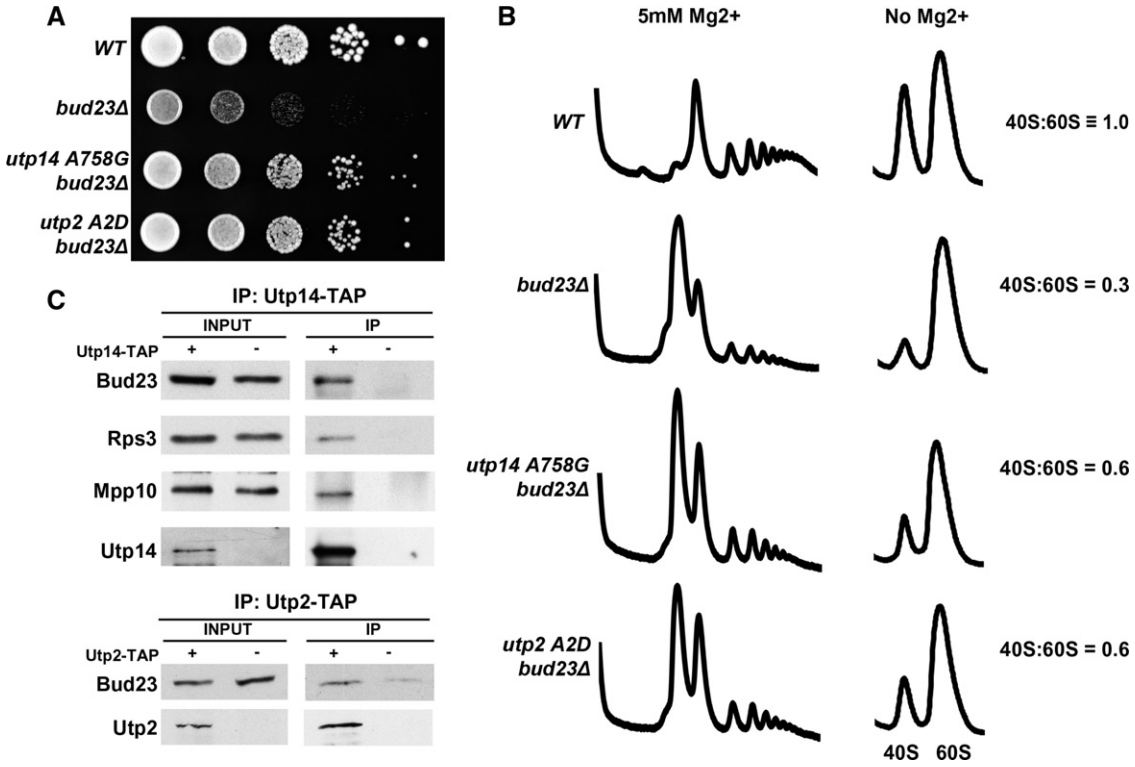

FIGURE 2. *bud23Δ* mutant is suppressed by mutations in the SSU processome proteins Utp14 and Utp2. (*A*) Tenfold serial dilutions of the isogenic wild type (BY4741), *bud23Δ* (AJY2161), *utp14-A758G bud23Δ* (AJY2683), and *utp2 A2D bud23Δ* (AJY3581) mutants were spotted on complete rich media (YPD) and incubated for 2 d at 30°C. (*B*) Point mutations in Utp14 or Utp2 improve the subunit balance in a *bud23Δ* mutant. Whole cell extracts from wild type, *bud23Δ*, *utp14-A758G bud23Δ*, and *utp2 A2D bud23Δ* strains were subjected to sucrose density gradient ultracentrifugation in the presence (5 mM) or absence of Mg^{2+}. Absorbance at 254 nm was monitored continuously throughout the gradients. (*C*) Bud23 coimmunoprecipitates with Utp14 and Utp2. Extracts from cells expressing Utp14-TAP or Utp2-TAP and myc-Bud23 were immunoprecipitated with IgG-Sepharose. Extracts from cells expressing only myc-Bud23 were used as negative control. Immunoprecipitated proteins were subjected to SDS-PAGE and Western blotting using anti-myc, anti-Rps3, anti-Mpp10, and peroxidase anti-peroxidase (PAP) to detect myc-Bud23, Rps3, Mpp10, and Utp14, respectively.

Utp2 proteins were expressed at levels similar to wild-type proteins, and increased dosage of wild-type genes did not suppress *bud23Δ* (data not shown), indicating that suppression was due to functional differences in the mutant proteins. Both Utp14 and Utp2/Nop14 have been previously described as essential SSU processome components (Dragon et al. 2002; Kuhn et al. 2009); however, they have not been assigned to any specific class of UTP proteins. Although it has been suggested that Utp14 is an ATPase (Phipps et al. 2011), the putative Walker-A motif is not conserved among Utp14 homologs, leading us to conclude that it is unlikely that Utp14 hydrolyzes ATP.

The genetic interaction between *BUD23* and *UTP14* and *UTP2* prompted us to ask whether they also exhibit physical interaction. To do this, we affinity-purified genomic TAP-tagged Utp14 and Utp2 and probed for Bud23, Rps3, a small subunit marker, and Mpp10, an SSU processome component, as controls. Bud23 copurified with both Utp14 and Utp2 (Fig. 2C). These results were somewhat unexpected, considering the lack of physical interaction between other Utp proteins and Bud23 observed in Figure 1, and suggest that either Bud23 transiently interacts with the 90S pre-ribosome or that some SSU processome components are retained on the pre-40S particle after cleavage at A2.

The absence of Bud23 results in a specific mislocalization of several UTP components

To investigate the functional significance of the genetic interaction of *BUD23* and *UTP14*, we asked if the deletion of *BUD23* affects the localization of SSU processome components. We arbitrarily chose genomic GFP-tagged Utp9, Utp10, Utp13, and Utp18 strains (Huh et al. 2003). All of these proteins were strongly nucleolar in localization in a wild-type background (Fig. 3A, left). However, in a *bud23Δ* mutant, these proteins were significantly enriched in the nucleoplasm, in addition to their nucleolar localization (Fig. 3A, right). A similar mislocalization was also observed for Utp14 (Fig. 3B). On the other hand, the U3 snoRNA, a core component of the SSU processome, did not display a change in localization in the absence of Bud23 (data not shown). This suggests that the mislocalization phenotype of UTP factors is independent of U3 snoRNA, possibly reflecting the mislocalization of a

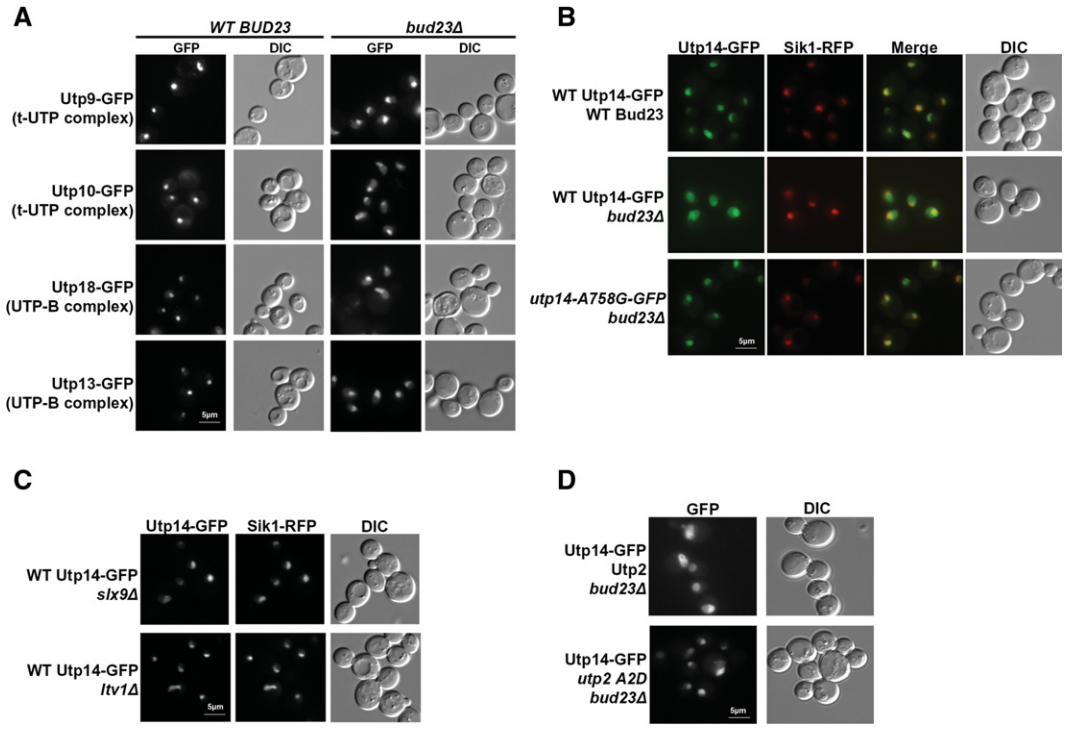

FIGURE 3. Bud23 is required for the proper localization of SSU components. (*A*) UTP proteins mislocalize to the nucleoplasm in the absence of Bud23. The indicated strains expressing genomic GFP-tagged proteins in a wild-type or *bud23Δ* background were grown in synthetic complete media to mid-log phase at 30°C and analyzed for GFP fluorescence and differential interference contrast (DIC). (*B*) A point mutation in Utp14 corrects the mislocalization in a *bud23Δ* mutant. Strains expressing wild-type (wt) Utp14-GFP wt Bud23 (AJY3261), wt Utp14-GFP *bud23Δ* (AJY3263), and *utp14-A758G-GFP bud23Δ* (AJY3262) were grown in synthetic complete media to mid-log phase at 30°C and analyzed for GFP fluorescence (green) and DIC. Sik1-RFP (pAJ1629) was used as a nucleolar marker (red). (*C*) Mislocalization of Utp14 is specific to a *bud23Δ* mutant. The indicated strains expressing Utp14-GFP in a *slx9Δ or ltv1Δ* background were grown in synthetic complete media to mid-log phase at 30°C and analyzed for Utp14-GFP fluorescence. (*D*) A point mutation in Utp2 (*utp2-A2D*) corrects the mislocalization of Utp14-GFP in a *bud23Δ* mutant. A *bud23Δ* strain expressing wt Utp14-GFP and containing wt Utp2 (pAJ2595) or *utp2-A2D* (pAJ2596) was grown in synthetic complete media to mid-log phase at 30°C and analyzed for Utp14-GFP localization.

specific subcomplex(es) of the processome. We also monitored the localization of Sik1-RFP as a nucleolar marker. Sik1-RFP localization remained largely restricted to the nucleolus in all the conditions tested. Hence, the mislocalization of Utp14 and other SSU components was not due to a gross change of nucleolar structure. To check if the aberrant nucleoplasmic localization of Utp14 is specific to a *bud23Δ* mutant or is a general defect associated with small subunit biogenesis mutants, we looked at the localization of Utp14-GFP in *ltv1Δ* and *slx9Δ* mutants. Ltv1 is a late-stage 40S biogenesis factor (Seiser et al. 2006), whereas Slx9 has been shown to be associated with the 90S pre-ribosome (Grandi et al. 2002; Bax et al. 2006). The localization of Utp14-GFP remained restricted to the nucleolus in both *ltv1Δ* and *slx9Δ* mutants (Fig. 3C). These results together suggest that the deletion of *BUD23* has a specific effect on the localization of SSU components.

The mislocalization of Utp14 in *bud23Δ* mutant cells was corrected by the *utp14-A758G* mutation (Fig. 3B, third panel). The mislocalization of Utp14 could also be corrected by expression of the dominant *utp2-A2D* mutant from a plasmid (Fig. 3D); 60% of the cells expressing *utp2-A2D* showed strictly nucleolar localization of Utp14-GFP compared with 13% in the presence of wild-type *UTP2*. Thus, mutations in Utp14 and Utp2 that suppress a *bud23Δ* mutant can correct the defect in localization of Utp14. These results strongly suggest that the mutations in *UTP2* and *UTP14* suppress *bud23Δ* by a common mechanism.

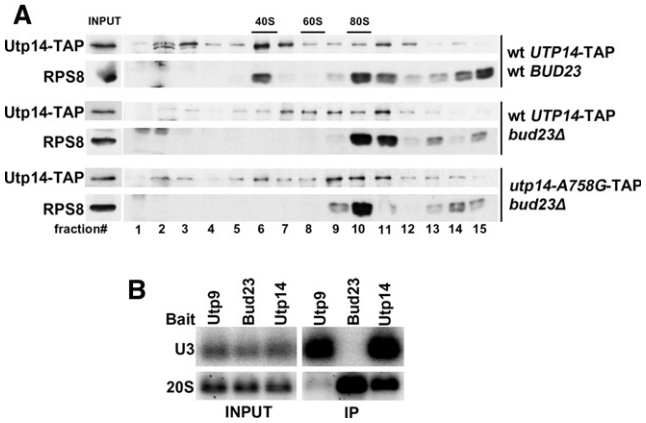

FIGURE 4. Utp14 sedimentation is perturbed in a *bud23Δ* mutant. (*A*) Utp14-TAP sediments with pre-40S and 90S pre-ribosomes. Whole cell extracts from cycloheximide-treated cells expressing genomic wt Utp14-TAP wt Bud23 (AJY3561), wt Utp14-TAP *bud23Δ* (AJY3528), *utp14-A758G-TAP bud23Δ* (AJY3532) were subjected to sucrose density gradient ultracentrifugation. Proteins were precipitated from fractions and subjected to SDS-PAGE. Utp14-TAP and Rps8 were detected using PAP and anti-Rps8 antibody, respectively. The positions of 40S, 60S, and 80S are indicated. The lower band in the *top* panel is a degradation product of Utp14-TAP. (*B*) Utp14-TAP immunoprecipitates U3 snoRNA as well as 20S pre-rRNA. Extracts from cells expressing Utp9-TAP, Bud23-TAP, or Utp14-TAP were immunoprecipitated with IgG-Sepharose. Immunoprecipitated RNA was analyzed for the presence of U3 snoRNA and 20S rRNA by Northern blotting with the oligos listed in Table 5.

UTP14 interacts with both 90S and pre-40S particles

Although classified as an SSU processome component, the function of Utp14 in small-subunit biogenesis is not known. To better understand which ribosomal precursors Utp14 interacts with, we monitored the sedimentation of Utp14-TAP on a sucrose gradient. We also monitored the sedimentation of Rps8 as a control for 40S, 80S, and polysomes. In wild-type cells, Utp14-TAP sedimented not only at the approximate position of 90S (Fig. 4A, top, fractions 10–12), as expected for an SSU processome factor, but also at the position of 40S/pre-40S (Fig. 4A, top, fraction 6). In fact, more Utp14 was observed at the position of 40S than at 90S. In the absence of Bud23, Utp14 sedimented with the 90S but was absent in the pre-40S region (Fig. 4A, middle). Instead, Utp14 appeared to sediment in higher-molecular-weight complexes at the approximate position of 60S (Fig. 4A, middle, fractions 7–9). The sedimentation pattern of *utp14-A758G-TAP* was intermediate between the sedimentation of Utp14-TAP in a wild-type (wt) and *bud23Δ* mutant, and the signal at the position of pre-40S is partially restored (Fig. 4A, bottom).

To confirm that the Utp14-TAP signal sedimenting at the position of pre-40S represents a pre-40S-associated particle, we asked if Utp14-TAP would immunoprecipitate 20S pre-rRNA. Indeed, Bud23 and Utp14, but not Utp9, pulled down 20S rRNA (Fig. 4B). However, both Utp14 and Utp9, but not Bud23 efficiently pulled down U3 snoRNA. Utp2 has also been previously shown to immunoprecipitate U3 snoRNA, as well as 35S and 20S pre-rRNAs (Dragon et al. 2002; Kühn 2007). This suggests that although Utp14 and Utp2 have been described as SSU processome components, they stay on the pre-40S particle at least until after the cleavage at A2 to form 20S pre-RNA.

Utp14 particle in a *bud23Δ* mutant contains U3 snoRNA but lacks 20S pre-rRNA

In a *bud23Δ* mutant, Utp14–TAP sedimented at the approximate position of 60S and was lost from the pre-40S position. We performed immunoprecipitations with Utp14–TAP in a wt and *bud23Δ* mutant to analyze the differences in Utp14-associated complexes. 20S rRNA was not detected in the Utp14–TAP complex in the absence of Bud23, but was partially restored in the *utp14-A758G* suppressor mutant (Fig. 5A). Consistent with 20S rRNA analysis, several ribosomal proteins including Rps3, Rps24, and Rps2 were significantly underrepresented in the Utp14–TAP particle in a *bud23Δ* mutant (Fig. 5C; data not shown). We also observed a modest reduction in SSU processome components Mpp10 and Imp4 (Fig. 5C), but did not see a reduction in the levels of U3 snoRNA associated with Utp14–TAP in the *bud23Δ* mutant (Fig. 5B). These results suggest that in the absence of Bud23, Utp14 and presumably some but not all SSU processome

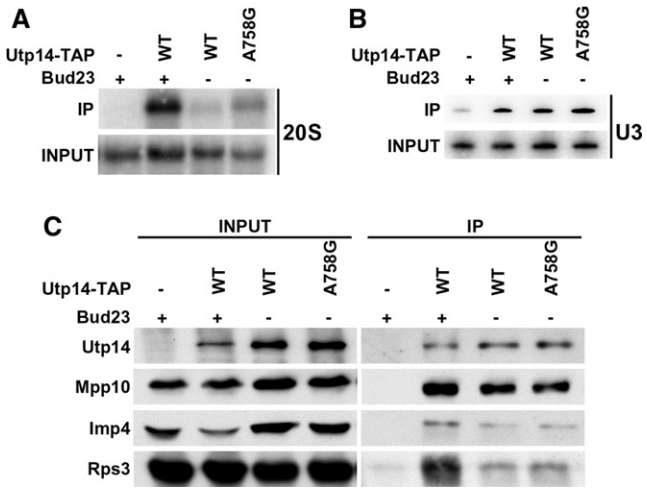

FIGURE 5. Utp14-containing particles contain U3 snoRNA but lack 20S or ribosomal proteins in a *bud23Δ* mutant. (*A*) Utp14–TAP does not immunoprecipitate 20S pre-rRNA in a *bud23Δ* mutant. Extracts from the indicated strains expressing wt Utp14–TAP wt Bud23 (AJY3561), wt Utp14–TAP *bud23Δ* (AJY3528), *utp14-A758G-TAP bud23Δ* (AJY3532) were immunoprecipitated with IgG-Sepharose. Extracts prepared from cells expressing untagged Utp14 were used as negative control. Immunoprecipitated RNA was analyzed for the presence of 20S by Northern blotting with the oligos listed in Table 5. (*B*) Utp14-TAP immunoprecipitates U3 snoRNA in a *bud23Δ* mutant. Extracts from the strains described in *A* were immunoprecipitated with IgG-Sepharose and analyzed for the presence of U3 snoRNA by Northern blotting with the oligos listed in Table 5. (*C*) Utp14–TAP immunoprecipitates less Mpp10, Imp4, and ribosomal proteins in a *bud23Δ* mutant. Extracts from the strains described in *A* were immunoprecipitated with IgG-Sepharose. Immunoprecipitated proteins were subjected to SDS-PAGE and Western blotting using PAP, anti-Mpp10, anti-Imp4, and anti-Rps3 antibodies to detect Utp14–TAP, Mpp10, Imp4, and Rps3, respectively.

components along with U3 snoRNA are trapped in a high-molecular-weight complex that sediments approximately at 60S but is not associated with 20S pre-rRNA or ribosomal proteins. The absence of 20S or other related rRNA species could be due to degradation of a stalled rRNA intermediate in this complex or reflect a subassembly of the SSU processome that accumulates separate from pre-rRNA in a *bud23Δ* mutant.

Bud23 is required for efficient A2 cleavage

We examined the steady-state levels of rRNA precursors in wt, *bud23Δ* mutant, and a suppressed *bud23Δ* mutant containing *utp14-A758G* or *utp2-A2D*. As we have shown previously (White et al. 2008), A2 cleavage in a *bud23Δ* mutant was inefficient, with a marked reduction in the levels of 27S A2 intermediate (Fig. 6A, lane 1). Interestingly, the *utp14-A758G* as well as *utp2-A2D* suppressors restored 27SA2 pre-rRNA in *bud23Δ* cells to levels intermediate between wild type and *bud23Δ* mutant, resulting in an overall improvement in 18S levels (Fig. 6A, lanes 3,4; quantified in Fig. 6C).

In the absence of A2 cleavage, cleavage at A3 is likely to be essential for separating the precursors for 40S and 60S processing. The strong negative genetic interaction that we observed between *bud23Δ* and RNase MRP components (Table 1) may reflect such a block in rRNA processing. Accordingly, we analyzed pre-rRNA processing in the double mutants by Northern hybridization. The negative genetic interaction between *bud23Δ* and the ts mutants was observed at 30°C, a temperature at which the single mutants are viable. We therefore analyzed rRNA processing in all strains at 30°C. Pop3 and Snm1 are essential components of RNase MRP, the primary activity responsible for cleavage at A3 (Lygerou et al. 1996). Not surprisingly, the double mutants of RNase MRP and *bud23Δ* had significantly reduced levels for 20S and 18S rRNAs, when normalized to U2 (Fig. 7A; quantified in Fig. 7B). Similar results were obtained in multiple experiments. This is consistent with simultaneously impairing A2 and A3 cleavage in the double mutant. The defects in cleavage at A2 and A3 are also reflected in the reduction in the total levels of 5.8S rRNA in the double mutants (Fig. 7C). In wild-type cells as well as *bud23Δ* mutant, A3 cleavage occurs normally, and $5.8S_S$ is the predominant form of 5.8S rRNA. Because A3 is the entry site for the nucleases responsible for processing the 5′ end of $5.8S_S$, a defect in A3 cleavage in RNase MRP mutants results in reduced production of $5.8S_S$ and results in a 30% reduction in the total levels of 5.8S ($5.8S_S + 5.8S_L$). However, the *bud23Δ* RNase MRP double mutants exhibited a more pronounced defect in 5.8S levels (60%–80% reduction) than either single mutant or the expected effect of the double mutants. Thus, the strong negative genetic interaction of these double mutants was likely due to reduced cleavage at

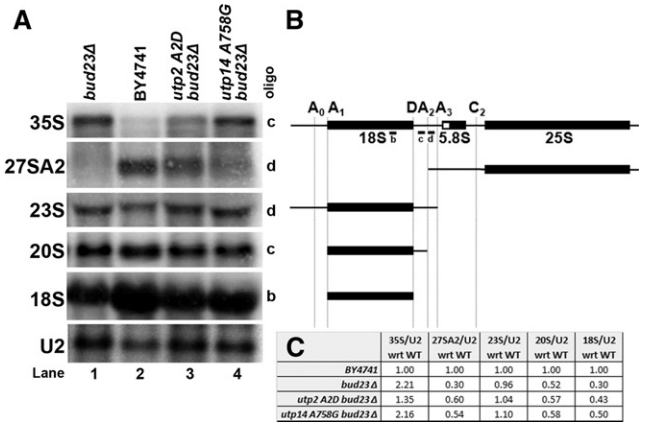

FIGURE 6. Suppressors of *bud23Δ* mutant restore A2 cleavage. (*A*) Total RNA extracted from the indicated strains grown to $OD_{600} \sim 0.3$ in YPD at 30°C was separated on an agarose/formaldehyde denaturing gel, transferred to a membrane, and probed with the indicated oligonucleotide probes to identify rRNA processing intermediates. U2 RNA was used as a loading control and probed with AJO962 listed in Table 5. (*B*) Schematic depicting pre-rRNA intermediates and probes used. (*C*) Quantitation of Northerns shown in *A*. The hybridization signals were detected by phosphorimaging and quantified using Quantity One (Bio-Rad).

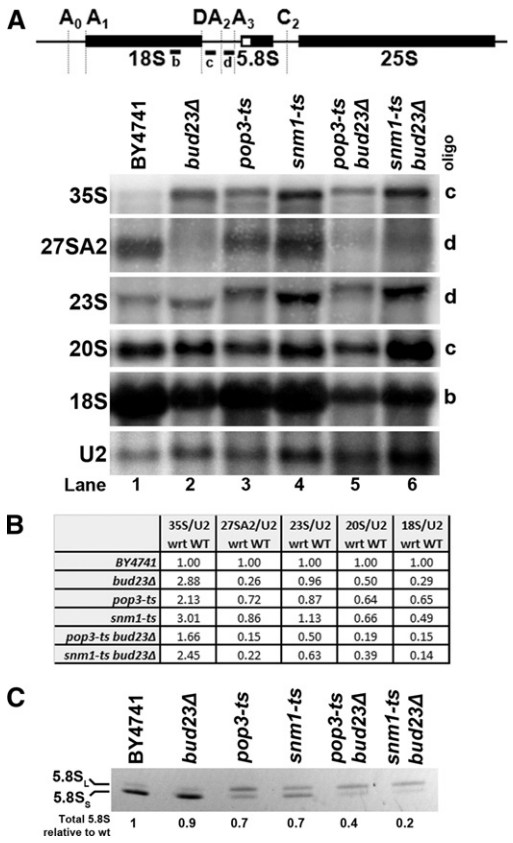

	35S/U2 wrt WT	27SA2/U2 wrt WT	23S/U2 wrt WT	20S/U2 wrt WT	18S/U2 wrt WT
BY4741	1.00	1.00	1.00	1.00	1.00
bud23Δ	2.88	0.26	0.96	0.50	0.29
pop3-ts	2.13	0.72	0.87	0.64	0.65
snm1-ts	3.01	0.86	1.13	0.66	0.49
pop3-ts bud23Δ	1.66	0.15	0.50	0.19	0.15
snm1-ts bud23Δ	2.45	0.22	0.63	0.39	0.14

FIGURE 7. Negative genetic interaction between BUD23 and RNase MRP mutants is due to a defect in A2 cleavage. (*A*) Total RNA extracted from the indicated strains grown to $OD_{600} \sim 0.3$ in YPD at 30°C was separated on an agarose/formaldehyde denaturing gel, transferred to a membrane, and probed with the indicated oligonucleotide probes to identify rRNA processing intermediates. U2 was probed as described in Figure 6. (*B*) Quantitation of the Northern blots shown in *A*. The hybridization signals were detected by phosphorimaging and quantified using Quantity One (Bio-Rad). (*C*) Levels of both $5.8S_S$ and $5.8S_L$ rRNAs are reduced in *bud23Δ rnaseMRP-ts* double mutants. Total RNA from strains described in *A* were resolved on a 10% TBE-urea polyacrylamide gel, visualized by staining with ethidium bromide and quantified using Image J (NIH). For quantitation of 5.8S levels, total $5.8S_S$ + $5.8S_L$ rRNA signal was normalized to tRNA (loading control) and represented as a ratio to the wild-type 5.8S level.

both A2, due to *bud23Δ*, and at A3, due to *pop3* or *snm1* ts mutations. A failure to cleave at A2 and A3 will result in an overall inability to properly process the pre-40S and a general failure in ribosome biogenesis.

DISCUSSION

BUD23 works at the transition of early to middle stage of 40S biogenesis

Biogenesis of the small ribosomal subunit is a dynamic process that can be divided into stages, marked by critical rRNA cleavages, key structural rearrangements, and the actively changing repertoire of accessory factors associated with the maturing ribosome (Schafer et al. 2003). On the basis of results presented here, we propose that Bud23 acts at the transition of early to middle stage of small subunit biogenesis, at the time of A2 cleavage and after the first two endonucleolytic cleavages in the 5′ ETS at A0 and A1. rRNA processing has been shown to proceed both by cotranscriptional and post-transcriptional cleavages of the nascent precursor 35S rRNA. High-resolution kinetic labeling studies have reported that ~70% of the nascent transcripts are cleaved cotranscriptionally at A2 (Kos and Tollervey 2010). We have previously shown an ~70% reduction in total 40S levels in a *bud23Δ* mutant (White et al. 2008). It is possible that Bud23 acts primarily in the cotranscriptional cleavage pathway of rRNA processing.

If Bud23 is required for efficient A2 cleavage, we would imagine that it should join the 90S particle before this cleavage event. Although Bud23 did copurify with Utp2 and Utp14, it did not copurify with other early SSU processome factors. This may be due to the transient nature of these interactions or concurrent disassembly of the SSU processome when Bud23 enters the particle. The behavior of Bud23 is reminiscent of another putative methyltransferase, Rrp8, that shows synthetic lethality with *gar1* mutants and strongly affects cleavage at A2 but does not immunoprecipitate SSU processome components or H/ACA or C/D box snoRNPs (Bousquet-Antonelli et al. 2000). However, how Rrp8 mediates its role in rRNA processing or its putative substrate is not understood.

Is Bud23 involved in disassembly of the SSU processome?

The dynamics of *trans*-acting factors coming into and leaving the pre-ribosomal particles during their assembly requires the coordinated recruitment and release of proteins. Many of these release events require GTPases or ATPases that are thought to drive conformational changes (Strunk and Karbstein 2009; Kressler et al. 2012). The genetic analysis of these events in the later steps of 60S biogenesis reveals a special relationship between *trans*-acting factors and their devoted releasing factors (Lo et al. 2010; Panse and Johnson 2010). In many cases, a requirement for a releasing factor can be bypassed by mutations in the target *trans*-acting factor that must be released. In these cases, the suppressing mutations weaken the affinity of the factor for the pre-60S particle (Senger et al. 2001; West et al. 2005). In the 40S pathway, we show that single-point mutations in Utp14 (*utp14-A758G*) or Utp2/Nop14 (*utp2-A2D*) result in suppression of A2 cleavage defect in a *bud23Δ* mutant, resulting in improved 40S production and improved growth. By analogy to the genetic interactions observed in the 60S pathway, we suggest that the suppressing mutations in *UTP14* and *UTP2* facilitate disassembly of complexes that fail to disassemble efficiently in the absence of Bud23. Because both

UTP14 and *UTP2* are essential, the suppressing mutations must maintain protein function while bypassing the lack of Bud23. However, we observed an increase of Utp14 sedimentation in the region of 60S instead of 40S in the absence of Bud23, suggesting an accumulation of an U3 snoRNA-containing aberrant or intermediate complex due to a defect in disassembly of some but not all processome factors.

The steady-state localization of most SSU processome and early pre-rRNA processing factors is nucleolar. However, work in human cells has demonstrated rapid exchange of factors involved in pre-rRNA processing between the nucleolus and nucleoplasm (Phair and Misteli 2000; Chen and Huang 2001; Leary et al. 2004). This was suggested to reflect recycling of these factors for subsequent rounds of processing in the nucleolus. According to this model, after the early processing cleavages at A0, A1, and A2, the SSU processome disassembles leaving ribosomal proteins and additional accessory factors required for later processing steps bound to the pre-rRNA. The processome components released into the nucleoplasm must then cycle back into the nucleolus for the next round of pre-rRNA processing (Leary and Huang 2001). A delay in disassembly of the complex in a *bud23Δ* mutant could result in a change in the steady-state distribution of these proteins as monitored by GFP localization.

We show that the deletion of *BUD23* results in steady-state enrichment of nucleoplasmic localization of several SSU processome components. Failure of timely disassembly of these components could lock these factors in dead-end intermediates and block their participation in subsequent rounds of pre-rRNA processing. We observed that Utp14 complexes in the absence of Bud23 lack several ribosomal proteins, possibly reflecting stalled assembly intermediates. The lack of disassembly may also be indirectly responsible for the nuclear export defect we earlier reported in a *bud23Δ* mutant (White et al. 2008).

Genetic interaction with RNase MRP

The RNase MRP components Pop3, Pop4, and Snm1 showed strong negative genetic interaction with *bud23Δ*. RNase MRP is an essential and evolutionarily conserved ribonucleoprotein complex that is responsible for the endonucleolytic cleavage at A3 in ITS1 (Lygerou et al. 1996). Mutations in both the RNA and protein components of RNase MRP have been implicated to result in a compromised immune system and dwarfism (Mattijssen et al. 2010). Cleavage at A3 initiates the formation of the 5′ end of 5.8S rRNA (Chu et al. 1994; Henry et al. 1994). However, cleavage of 35S rRNA by RNase MRP at A3 can presumably still continue even in the absence of A1/A2 cleavage (Henry et al. 1994; Torchet et al. 1998; Torchet and Hermann-Le Denmat 2000). A *bud23Δ* mutant by itself is severely compromised for A2 cleavage and is probably largely dependent on cotranscriptional A3 cleavage by RNase MRP to release the pre-40S particle. We suggest that the simultaneous blocks in cleavage at A2 and A3 in the *bud23Δ rnase MRP-ts* double mutant, accounts for the severe negative genetic interaction.

Does Bud23 monitor pre-40S assembly to trigger A2 cleavage?

Our work provides evidence for a role of Bud23 in the transition of the small subunit from an early 90S particle to a middle-stage pre-40S particle. This transition is marked by several key and interdependent events: formation of the central pseudo-knot, cleavage at A2 in ITS1, and the removal of several early SSU processome components from the pre-ribosome to allow for subsequent maturation (Schafer et al. 2003; Henras et al. 2008). The central pseudoknot is the key architectural feature of the overall RNA structure of the small subunit. The correct folding of the central pseudoknot is thought to set the stage for A2 cleavage leading to the separation of 40S and 60S maturation pathways. Mutants that cannot stably form the central pseudoknot are thought to be defective for cleavage at A2 resulting in the absence of a detectable 27SA2 pre-rRNA intermediate (Beltrame and Tollervey 1995; Hughes 1996).

Bud23 methylates G1575 in 18S rRNA in a helix that stacks coaxially with the central pseudoknot. We have shown previously that Bud23 protein, but not its methyltransferase activity, is important for its function (White et al. 2008). Considering the physical relationship between the Bud23 methylation site and the central pseudoknot, we propose that recognition of its substrate by Bud23 may be a means of monitoring the status of assembly of the small subunit. In this model, we imagine that Bud23 triggers cleavage at A2 only after correct folding of its substrate, which may depend on the completion of the folding of the central pseudoknot. Methylation of its target site may then simply be a means of "marking" the subunit as having passed a quality-control checkpoint.

MATERIALS AND METHODS

Strains, plasmids, and media

All *S. cerevisiae* strains used in this study are listed in Table 3. All TAP-tagged and GFP-tagged strains were from Open Biosystems and temperature-sensitive strains were kindly provided by Dr. P. Hieter (Ben-Aroya et al. 2008).

Identification of utp14-A758G suppressor and construction of bud23Δ suppressor library

Ten micrograms of total yeast DNA was partially digested with Sau3A1 and then size-fractionated on a 10%–40% sucrose gradient prepared in 1 M NaCl, 20 mM Tris-HCl (pH 7.5), 5 mM EDTA by centrifugation at 30,000 rpm for 20 h at 20°C in a SW40 rotor (Beckman). DNA was extracted from fractions containing 1- to 3-kb DNA fragments and was cloned into the BamHI site of pRS416. The library was transformed into a *bud23Δ* mutant and screened

TABLE 3. Strains used in this study

Strain	Genotype	Source
AJY2161	*MATa bud23Δ::KanMX his3Δ1 leu2Δ0 ura3Δ0 met15Δ0*	White et al. 2008
AJY2643	*MATa his3Δ1 leu2Δ0 met15Δ0 ura3Δ0*	Winzeler et al. 1999
AJY2665	*MATa ENP1-TAP::HIS3MX6 leu2Δ0 ura3Δ0*	Ghaemmaghami et al. 2003
AJY2666	*MATa NOB1-TAP::HIS3MX6 leu2Δ0 ura3Δ0*	Ghaemmaghami et al. 2003
AJY2667	*MATa RIO2-TAP::HIS3MX6 leu2Δ0 ura3Δ0*	Ghaemmaghami et al. 2003
AJY2683	*MATa bud23Δ::NatMX utp14-A758G his3Δ1 leu2Δ0 ura3Δ0*	This study
AJY2891	*MATa LTV1-TAP::HIS3MX6 leu2Δ0 ura3Δ0*	Ghaemmaghami et al. 2003
AJY2897	*MATa HRR25-TAP::HIS3MX6 leu2Δ0 ura3Δ0*	Ghaemmaghami et al. 2003
AJY3128	*MAT*[a] *pop3-ts::URA3 bud23Δ::KanMX his3Δ1 leu2Δ0*	This study
AJY3129	*MAT*[a] *snm1-ts::URA3 bud23Δ::KanMX his3Δ1 leu2Δ0*	This study
AJY3255	*MATa ura3Δ0 leu2Δ0 his3Δ1 lys2Δ0* (or LYS2) *met15Δ0* (or MET15) *can1Δ::LEU2-MFA1pr::His3 pop3-ts::URA3*	Ben-Aroya et al. 2008
AJY3259	*MATa ura3Δ0 leu2Δ0 his3Δ1 lys2Δ0* (or LYS2) *met15Δ0* (or MET15) *can1Δ::LEU2-MFA1pr::His3 snm1-ts::URA3*	Ben-Aroya et al. 2008
AJY3261	*MATa UTP14-GFP::HIS3MX6 leu2Δ0 ura3Δ0*	Huh et al. 2003
AJY3262	*MATa utp14-A758G-GFP::HIS3MX6 bud23Δ::NatMX leu2Δ0 ura3Δ0*	This study
AJY3263	*MATa UTP14-GFP::HIS3MX6 bud23Δ::KanMX leu2Δ0 ura3Δ0*	This study
AJY3317	*MATa UTP2-TAP::KlURA3 his3Δ1 leu2Δ0 met15Δ0*	This study
AJY3431	*MATa UTP9-GFP::HIS3MX6 leu2Δ0 ura3Δ0*	Huh et al. 2003
AJY3434	*MATa UTP18-GFP::HIS3MX6 leu2Δ0 ura3Δ0*	Huh et al. 2003
AJY3436	*MATa UTP10-GFP::HIS3MX6 leu2Δ0 ura3Δ0*	Huh et al. 2003
AJY3437	*MATa UTP13-GFP::HIS3MX6 leu2Δ0 ura3Δ0*	Huh et al. 2003
AJY3440	*MATa UTP9-GFP::HIS3MX6 bud23Δ::KanMX leu2Δ0 ura3Δ0*	This study
AJY3442	*MATa UTP10-GFP::HIS3MX6 bud23Δ::KanMX leu2Δ0 ura3Δ0*	This study
AJY3443	*MATa UTP18-GFP::HIS3MX6 bud23Δ::KanMX leu2Δ0 ura3Δ0*	This study
AJY3444	*MATa UTP13-GFP::HIS3MX6 bud23Δ::KanMX leu2Δ0 ura3Δ0*	This study
AJY3501	*MATa UTP9-TAP::HIS3MX6 leu2Δ0 ura3Δ0*	Ghaemmaghami et al. 2003
AJY3503	*MATa UTP22-TAP::HIS3MX6 leu2Δ0 ura3Δ0*	Ghaemmaghami et al. 2003
AJY3504	*MATa UTP25-TAP::HIS3MX6 leu2Δ0 ura3Δ0*	Ghaemmaghami et al. 2003
AJY3506	*MATa UTP18-TAP::HIS3MX6 leu2Δ0 ura3Δ0*	Ghaemmaghami et al. 2003
AJY3510	*MATa HCR1-TAP::HIS3MX6 leu2Δ0 ura3Δ0*	Ghaemmaghami et al. 2003
AJY3518	*MATa UTP14-GFP::HIS3MX6 slx9Δ::KanMX leu2Δ0 ura3Δ0*	This study
AJY3519	*MATa UTP14-GFP::HIS3MX6 ltv1Δ:KanMX leu2Δ0 ura3Δ0*	This study
AJY3528	*MATa UTP14-TAP::KlURA3 bud23Δ::KanMX his3Δ1 leu2Δ0 met15Δ0*	This study
AJY3532	*MATa utp14-A758G-TAP::KlURA3 bud23Δ::KanMX his3Δ1 leu2Δ0 met15Δ0*	This study
AJY3560	*MATa UTP14-TAP::KlURA3 his3Δ1 leu2Δ0 met15Δ0*	This study
AJY3581	*MATa bud23Δ::KanMX utp2-A2D his3Δ1 leu2Δ0 met15Δ0 ura3Δ0*	This study

[a]Mating type not determined.

for suppressing phenotype. The plasmid harboring the dominant suppressor was isolated and the insert identified by sequencing.

Identification of utp2-A2D suppressor

The suppressing mutation was identified by high-throughput SOLiD sequencing of the suppressor genomic DNA. Sequencing was carried out by the Genome Sequencing and Analysis Facility at UT Austin.

Construction of strains for the genetic screen

A subset of temperature-sensitive mutant strains (Ben-Aroya et al. 2008) was mated with a *bud23Δ* strain, sporulated, and dissected at room temperature. For quantification of genetic interactions, cells were cultured in 100 µL of YPD containing 75 µg/mL Ampicillin in 96-well plates by shaking continuously for 36 h in a microplate reader (Powerwave; Biotek). The doubling times were calculated from growth curves as described (Toussaint and Conconi 2006). The fitness of each strain was calculated as the ratio of the doubling time of the wild type to that of the mutant (Dixon et al. 2009). The expected fitness of double mutants was calculated as the product of the observed fitness of the parental single-mutant strains. For quantitation of negative genetic interaction, growth was monitored at 31°C where the ts mutants were viable but exhibited a fitness defect. Fitness reduction was calculated as a percentage of the difference between expected and observed fitness values. For quantitation of positive genetic interaction, growth was monitored at 33°C, where the ts mutants exhibited a significant fitness defect to measure improvement in fitness. Fitness improvement was calculated as a percentage of the difference between observed and expected fitness values.

Genomic integration of TAP tag at the C terminus of Utp14 and Utp2 was performed as described (Longtine et al. 1998). Swapping of the *HIS3MX6*-TAP cassette with the *KlURA3-HA* cassette was carried out as described (Sung et al. 2008). For deletion of the *BUD23* locus from GFP-tagged strains, the *bud23Δ::KanMX* cassette was amplified from AJY2161 and transformed into the parent GFP-tagged strains. All strains constructed by homologous recombination were confirmed by PCR.

Cells were cultured at 30°C, unless otherwise indicated, in rich medium or synthetic dropout medium, containing 2% glucose. All microbiological techniques and cloning were performed as described (Sambrook et al. 1989). Plasmids used in this study are listed in Table 4.

Immunoprecipitation and Western blotting

For immunoprecipitations, 200-mL cultures were grown to an OD_{600} of 0.6–0.8 in selective medium. Cells were resuspended in 500 µL of IP buffer (100 mM NaCl, 50 mM Tris-HCl at pH 7.5, 1.5 mM MgCl2, 0.15% NP-40, 1 mM PMSF, 1 µg/mL leupeptin, 1 µg/mL pepstatin A), lysed by vortexing with glass beads (five cycles of 30 sec of vortexing and 2 min on ice), and clarified by centrifugation at 15,000*g* at 4°C. Immunoprecipitation was performed for the protein A tag by incubating extracts with IgG-Sepharose beads (Amersham IgG Sepharose 6 Fast Flow) for 1 h at 4°C, followed by TEV enzyme cleavage for 2 h at 16°C. The beads were separated from the TEV eluate by centrifugation at 2000*g* for 30 sec. The eluted proteins in the supernatant were precipitated by adding 10% TCA and incubated overnight at −20°C. This was followed by centrifugation at 15,000*g* for 10 min at 4°C. The precipitated proteins were resuspended in 30 µL of 1× Laemmli buffer, heated for 5 min at 99°C, and separated on a 8% SDS-PAGE gel.

For Western blotting, membranes were incubated with the appropriate primary antibody for 2 h at room temperature or at 4°C overnight, and the secondary antibody for 30 min at room temperature.

Sucrose density gradient sedimentation

For polysome profile analysis, 200-mL cultures were grown at 30°C to OD_{600} of 0.3. Cycloheximide was added to the cultures (100 µg/mL final concentration) followed by incubation with shaking for 10 min at 30°C. The cells were then poured onto ice and collected by centrifugation. All subsequent steps were carried out 0°C–4°C. Cells were washed and resuspended in 600 µL of lysis buffer (100 mM KCl, 50 mM Tris-HCl at pH 7.5, 5 mM $MgCl_2$, 150 µg/mL cycloheximide, 7 mM BME, 1 mM PMSF, 1 µg/mL leupeptin, 1 µg/mL pepstatin A), and lysed by vortexing in the presence of glass beads. The extract was centrifuged for 10 min at 15,000*g* at 4°C, and the supernatant was recovered. Nine OD_{260} units were loaded onto a 7%–47% sucrose gradient prepared in lysis buffer and centrifuged for 2.5 h at 40,000 rpm (Beckman SW40 rotor). A gradient fractionator (ISCO Model 640) was used to record the UV profile and to collect fractions for further analysis.

TABLE 4. Plasmids used in this study

Plasmid	Description	Source
pAJ1629	*SIK1-mRFP MET15 CEN ARS*	Z Li and EM Marcotte, unpubl.
pAJ2151	*BUD23-GFP LEU2 CEN ARS*	White et al. 2008
pAJ2558	*BUD23-TAP LEU2 CEN ARS*	This study
pAJ2595	*wt Utp2 URA3 CEN ARS*	This study
pAJ2596	*utp2-A2D URA3 CEN ARS*	This study
pAJ2892	*Gal4BD-cmyc-Bud23 LEU2 2µ*	This study
pAJ2946	*13myc-BUD23 LEU2 CEN ARS*	This study

TABLE 5. Oligonucleotides used in this study

AJO	Target	Sequence
603	27SA2, 23S	TGTTACCTCTGGGCCCCGATTG
130	35S, 20S	TCTTGCCCAGTAAAAGCTCTCATGC
190	18S	GTCTGGACCTGGTGAGTTTCCC
962	U2	GCGACCAAAGTAAAAGTCAAGAAC GACTCCACAAGTGCGAGGGTCGCGAC
1686	U3	TAGATTCAATTTCGGTTTCTC

Microscopy

Overnight cultures were diluted to an OD_{600} of 0.1 into fresh selective medium and allowed to grow for 4–5 h at 30°C. Fluorescence was visualized on a Nikon E800 microscope fitted with a Plan Apo 100×/1.4 objective and a Photometrics CoolSNAP ES camera controlled by NIS-Elements AR2.10 software. Images were prepared using Adobe Photoshop CS5.

Northern blotting

All RNAs were prepared using acid phenol:chloroform extraction as described (Sambrook et al. 1989). The RNA species were separated by 1% agarose-formaldehyde gel electrophoresis and transferred to Zeta-Probe GT membrane (Bio-Rad) by capillary transfer. Dot blotting was performed by depositing 1% of the input RNA and one-third of the immunoprecipitated RNA onto a Zeta-Probe GT membrane (Bio-Rad) using a 96-well dot-blot system (Schleicher & Schuell). The transferred RNAs were UV-cross-linked to the membrane and Northern blotting using 5′-^{32}P-labeled oligonucleotide probes was performed as described previously (Li et al. 2009). The hybridization signals were detected by phosphorimaging and quantified using Quantity One (Bio-Rad). Oligonucleotides used in this study are listed in Table 5. U3 snoRNA and 5.8S rRNAs shown in Figure 7 were resolved on a 10% TBE-urea polyacrylamide gel (Life Technologies). 5.8S rRNAs were visualized by staining with ethidium bromide, and the signals were quantified using ImageJ (NIH).

ACKNOWLEDGMENTS

We thank S. Baserga for anti-Mpp10 and anti-Imp4, G. Dieci for anti-Rps8, M. Seedorf for anti-Rps3 antibodies, and Z. Li for Sik1-mRFP plasmid. This work was supported by NIH grant GM53655 to A.J.

Received December 10, 2012; accepted March 14, 2013.

REFERENCES

Bax R, Raue HA, Vos JC. 2006. Slx9p facilitates efficient ITS1 processing of pre-rRNA in *Saccharomyces cerevisiae*. *RNA* **12:** 2005–2013.

Beltrame M, Tollervey D. 1995. Base pairing between U3 and the pre-ribosomal RNA is required for 18S rRNA synthesis. *EMBO J* **14:** 4350–4356.

Ben-Aroya S, Coombes C, Kwok T, O'Donnell KA, Boeke JD, Hieter P. 2008. Toward a comprehensive temperature-sensitive mutant repository of the essential genes of *Saccharomyces cerevisiae*. *Mol Cell* **30:** 248–258.

Bousquet-Antonelli C, Vanrobays E, Gelugne JP, Caizergues-Ferrer M, Henry Y. 2000. Rrp8p is a yeast nucleolar protein functionally linked

to Gar1p and involved in pre-rRNA cleavage at site A2. *RNA* **6:** 826–843.

Chen D, Huang S. 2001. Nucleolar components involved in ribosome biogenesis cycle between the nucleolus and nucleoplasm in interphase cells. *J Cell Biol* **153:** 169–176.

Chu S, Archer RH, Zengel JM, Lindahl L. 1994. The RNA of RNase MRP is required for normal processing of ribosomal RNA. *Proc Natl Acad Sci* **91:** 659–663.

Dez C, Tollervey D. 2004. Ribosome synthesis meets the cell cycle. *Curr Opin Microbiol* **7:** 631–637.

Dixon SJ, Costanzo M, Baryshnikova A, Andrews B, Boone C. 2009. Systematic mapping of genetic interaction networks. *Annu Rev Genet* **43:** 601–625.

Dragon F, Gallagher JE, Compagnone-Post PA, Mitchell BM, Porwancher KA, Wehner KA, Wormsley S, Settlage RE, Shabanowitz J, Osheim Y, et al. 2002. A large nucleolar U3 ribonucleoprotein required for 18S ribosomal RNA biogenesis. *Nature* **417:** 967–970.

Figaro S, Wacheul L, Schillewaert S, Graille M, Huvelle E, Mongeard R, Zorbas C, Lafontaine DL, Heurgue-Hamard V. 2012. Trm112 is required for Bud23-mediated methylation of the 18S rRNA at position G1575. *Mol Cell Biol* **32:** 2254–2267.

French SL, Osheim YN, Cioci F, Nomura M, Beyer AL. 2003. In exponentially growing *Saccharomyces cerevisiae* cells, rRNA synthesis is determined by the summed RNA polymerase I loading rate rather than by the number of active genes. *Mol Cell Biol* **23:** 1558–1568.

Fromont-Racine M, Senger B, Saveanu C, Fasiolo F. 2003. Ribosome assembly in eukaryotes. *Gene* **313:** 17–42.

Gallagher JE, Dunbar DA, Granneman S, Mitchell BM, Osheim Y, Beyer AL, Baserga SJ. 2004. RNA polymerase I transcription and pre-rRNA processing are linked by specific SSU processome components. *Genes Dev* **18:** 2506–2517.

Ghaemmaghami S, Huh WK, Bower K, Howson RW, Belle A, Dephoure N, O'Shea EK, Weissman JS. 2003. Global analysis of protein expression in yeast. *Nature* **425:** 737–741.

Grandi P, Rybin V, Bassler J, Petfalski E, Strauss D, Marzioch M, Schafer T, Kuster B, Tschochner H, Tollervey D, et al. 2002. 90S pre-ribosomes include the 35S pre-rRNA, the U3 snoRNP, and 40S subunit processing factors but predominantly lack 60S synthesis factors. *Mol Cell* **10:** 105–115.

Granneman S, Baserga SJ. 2004. Ribosome biogenesis: Of knobs and RNA processing. *Exp Cell Res* **296:** 43–50.

Granneman S, Baserga SJ. 2005. Crosstalk in gene expression: Coupling and co-regulation of rDNA transcription, pre-ribosome assembly and pre-rRNA processing. *Curr Opin Cell Biol* **17:** 281–286.

Henras AK, Soudet J, Gerus M, Lebaron S, Caizergues-Ferrer M, Mougin A, Henry Y. 2008. The post-transcriptional steps of eukaryotic ribosome biogenesis. *Cell Mol Life Sci* **65:** 2334–2359.

Henry Y, Wood H, Morrissey JP, Petfalski E, Kearsey S, Tollervey D. 1994. The 5′ end of yeast 5.8S rRNA is generated by exonucleases from an upstream cleavage site. *EMBO J* **13:** 2452–2463.

Hughes JM. 1996. Functional base-pairing interaction between highly conserved elements of U3 small nucleolar RNA and the small ribosomal subunit RNA. *J Mol Biol* **259:** 645–654.

Huh WK, Falvo JV, Gerke LC, Carroll AS, Howson RW, Weissman JS, O'Shea EK. 2003. Global analysis of protein localization in budding yeast. *Nature* **425:** 686–691.

Kos M, Tollervey D. 2010. Yeast pre-rRNA processing and modification occur cotranscriptionally. *Mol Cell* **37:** 809–820.

Kressler D, Hurt E, Bergler H, Bassler J. 2012. The power of AAA-ATPases on the road of pre-60S ribosome maturation—molecular machines that strip pre-ribosomal particles. *Biochim Biophys Acta* **1823:** 92–100.

Kühn H. 2007. "Funktionelle Charakterisierung von Noc4p-Interaktionen in der Ribosomenbiogenese." PhD thesis, University of Regensburg, Regensburg, Germany.

Kuhn H, Hierlmeier T, Merl J, Jakob S, Aguissa-Toure AH, Milkereit P, Tschochner H. 2009. The Noc-domain containing C-terminus of Noc4p mediates both formation of the Noc4p-Nop14p submodule and its incorporation into the SSU processome. *PLoS ONE* **4:** e8370.

Leary DJ, Huang S. 2001. Regulation of ribosome biogenesis within the nucleolus. *FEBS Lett* **509:** 145–150.

Leary DJ, Terns MP, Huang S. 2004. Components of U3 snoRNA-containing complexes shuttle between nuclei and the cytoplasm and differentially localize in nucleoli: Implications for assembly and function. *Mol Biol Cell* **15:** 281–293.

Li Z, Lee I, Moradi E, Hung NJ, Johnson AW, Marcotte EM. 2009. Rational extension of the ribosome biogenesis pathway using network-guided genetics. *PLoS Biol* **7:** e1000213.

Lo KY, Li Z, Bussiere C, Bresson S, Marcotte EM, Johnson AW. 2010. Defining the pathway of cytoplasmic maturation of the 60S ribosomal subunit. *Mol Cell* **39:** 196–208.

Longtine MS, McKenzie A III, Demarini DJ, Shah NG, Wach A, Brachat A, Philippsen P, Pringle JR. 1998. Additional modules for versatile and economical PCR-based gene deletion and modification in *Saccharomyces cerevisiae*. *Yeast* **14:** 953–961.

Lygerou Z, Allmang C, Tollervey D, Seraphin B. 1996. Accurate processing of a eukaryotic precursor ribosomal RNA by ribonuclease MRP in vitro. *Science* **272:** 268–270.

Mattijssen S, Welting TJ, Pruijn GJ. 2010. RNase MRP and disease. *Wiley Interdiscip Rev RNA* **1:** 102–116.

Mougey EB, O'Reilly M, Osheim Y, Miller OL Jr, Beyer A, Sollner-Webb B. 1993. The terminal balls characteristic of eukaryotic rRNA transcription units in chromatin spreads are rRNA processing complexes. *Genes Dev* **7:** 1609–1619.

Osheim YN, French SL, Keck KM, Champion EA, Spasov K, Dragon F, Baserga SJ, Beyer AL. 2004. Pre-18S ribosomal RNA is structurally compacted into the SSU processome prior to being cleaved from nascent transcripts in *Saccharomyces cerevisiae*. *Mol Cell* **16:** 943–954.

Panse VG, Johnson AW. 2010. Maturation of eukaryotic ribosomes: Acquisition of functionality. *Trends Biochem Sci* **35:** 260–266.

Phair RD, Misteli T. 2000. High mobility of proteins in the mammalian cell nucleus. *Nature* **404:** 604–609.

Phipps KR, Charette J, Baserga SJ. 2011. The small subunit processome in ribosome biogenesis—progress and prospects. *Wiley Interdiscip Rev RNA* **2:** 1–21.

Sambrook J, Fritsch EF, Maniatis T. 1989. *Molecular cloning: A laboratory manual*. Cold Spring Harbor Laboratory Press, Cold Spring Harbor, NY.

Sardana R, Johnson AW. 2012. The methyltransferase adaptor protein Trm112 is involved in biogenesis of both ribosomal subunits. *Mol Biol Cell* **23:** 4313–4322.

Schafer T, Strauss D, Petfalski E, Tollervey D, Hurt E. 2003. The path from nucleolar 90S to cytoplasmic 40S pre-ribosomes. *EMBO J* **22:** 1370–1380.

Seiser RM, Sundberg AE, Wollam BJ, Zobel-Thropp P, Baldwin K, Spector MD, Lycan DE. 2006. Ltv1 is required for efficient nuclear export of the ribosomal small subunit in *Saccharomyces cerevisiae*. *Genetics* **174:** 679–691.

Senger B, Lafontaine DL, Graindorge JS, Gadal O, Camasses A, Sanni A, Garnier JM, Breitenbach M, Hurt E, Fasiolo F. 2001. The nucle(ol)ar Tif6p and Efl1p are required for a late cytoplasmic step of ribosome synthesis. *Mol Cell* **8:** 1363–1373.

Strunk BS, Karbstein K. 2009. Powering through ribosome assembly. *RNA* **15:** 2083–2104.

Sung MK, Ha CW, Huh WK. 2008. A vector system for efficient and economical switching of C-terminal epitope tags in *Saccharomyces cerevisiae*. *Yeast* **25:** 301–311.

Torchet C, Hermann-Le Denmat S. 2000. Bypassing the rRNA processing endonucleolytic cleavage at site A2 in *Saccharomyces cerevisiae*. *RNA* **6:** 1498–1508.

Torchet C, Jacq C, Hermann-Le Denmat S. 1998. Two mutant forms of the S1/TPR-containing protein Rrp5p affect the 18S rRNA synthesis in *Saccharomyces cerevisiae*. *RNA* **4:** 1636–1652.

Toussaint M, Conconi A. 2006. High-throughput and sensitive assay to measure yeast cell growth: A bench protocol for testing genotoxic agents. *Nat Protoc* **1:** 1922–1928.

Vanrobays E, Gelugne JP, Gleizes PE, Caizergues-Ferrer M. 2003. Late cytoplasmic maturation of the small ribosomal subunit requires RIO proteins in *Saccharomyces cerevisiae*. *Mol Cell Biol* **23:** 2083–2095.

Venema J, Tollervey D. 1999. Ribosome synthesis in *Saccharomyces cerevisiae*. *Annu Rev Genet* **33:** 261–311.

Vos HR, Faber AW, de Gier MD, Vos JC, Raue HA. 2004. Deletion of the three distal S1 motifs of *Saccharomyces cerevisiae* Rrp5p abolishes pre-rRNA processing at site A_2 without reducing the production of functional 40S subunits. *Eukaryot Cell* **3:** 1504–1512.

Warner JR. 2001. Nascent ribosomes. *Cell* **107:** 133–136.

Wery M, Ruidant S, Schillewaert S, Lepore N, Lafontaine DL. 2009. The nuclear poly(A) polymerase and Exosome cofactor Trf5 is recruited cotranscriptionally to nucleolar surveillance. *RNA* **15:** 406–419.

West M, Hedges JB, Chen A, Johnson AW. 2005. Defining the order in which Nmd3p and Rpl10p load onto nascent 60S ribosomal subunits. *Mol Cell Biol* **25:** 3802–3813.

White J, Li Z, Sardana R, Bujnicki JM, Marcotte EM, Johnson AW. 2008. Bud23 methylates G1575 of 18S rRNA and is required for efficient nuclear export of pre-40S subunits. *Mol Cell Biol* **28:** 3151–3161.

Winzeler EA, Shoemaker DD, Astromoff A, Liang H, Anderson K, Andre B, Bangham R, Benito R, Boeke JD, Bussey H, et al. 1999. Functional characterization of the *S. cerevisiae* genome by gene deletion and parallel analysis. *Science* **285:** 901–906.